

KINEMATICS OF OUTER HALO GLOBULAR CLUSTERS IN M31

J. VELJANOSKI¹, A.M.N. FERGUSON^{1,11}, A.D. MACKEY², A.P. HUXOR³, M.J. IRWIN⁴, P. CÔTÉ^{5,11}, N.R. TANVIR⁶, E. J. BERNARD¹, S. C. CHAPMAN⁴, R. A. IBATA⁷, M. FARDAL⁸, G. F. LEWIS⁹, N. F. MARTIN^{7,10}, A. MCCONNACHIE⁶ AND J. PEÑARRUBIA¹

Draft version August 17, 2021

ABSTRACT

We present the first kinematic analysis of the far outer halo globular cluster (GC) population in the Local Group galaxy M31. Our sample contains 53 objects with projected radii of $\sim 20-130$ kpc, of which 44 have no previous spectroscopic information. GCs with projected radii $\gtrsim 30$ kpc are found to exhibit net rotation around the minor axis of M31, in the same sense as the inner GCs, albeit with a smaller amplitude of 79 ± 19 km/s. The rotation-corrected velocity dispersion of the full halo GC sample is 106 ± 12 km/s, which we observe to decrease with increasing projected radius. We find compelling evidence for kinematic-coherence amongst GCs which project on top of halo substructure, including a clear signature of infall for GCs lying along the North-West stream. Using the tracer mass estimator, we estimate the dynamical mass of M31 within 200 kpc to be $M_{M31} = (1.2-1.5) \pm 0.2 \times 10^{12} M_{\odot}$. This value is highly dependent on the chosen model and assumptions within.

Subject headings: Local Group — galaxies: individual (M31) — galaxies: kinematics and dynamics — galaxies: halos — globular clusters: general

1. INTRODUCTION

Globular cluster (GC) systems contain important clues about the assembly history of galaxies (e.g., West et al. 2004). Their kinematics are especially important as different formation channels lead to distinct predictions (e.g. Forbes et al. 1997; Brodie & Strader 2006). Moreover, GC kinematics can also be used to model the shape of the gravitational potential and constrain the total mass of the host galaxy (e.g. Côté et al. 2001).

Located at a distance of ~ 780 kpc (McConnachie et al. 2005), the Local Group galaxy M31 provides an excellent opportunity to study a rich GC system in unparalleled detail. It has more than 500 confirmed members listed in the Revised Bologna Catalogue (RBC, Galleti et al. 2004), most of which lie within a projected radius (R_{proj}) of 30 kpc. In recent years, state-of-the-art wide field surveys (e.g. Ferguson et al. 2002; Ibata et al. 2007; McConnachie et al. 2009) have enabled searches for GCs in M31’s far outer halo. This has

led to the discovery of over 90 new halo GCs, extending to $R_{proj} \sim 140$ kpc and 3D radii of $\gtrsim 200$ kpc (e.g. Huxor et al. 2005; Huxor et al. 2008; Huxor et al. 2013, di Tullio Zinn & Zinn 2013). A major step forward in understanding the formation of the outer halo GC system came from the realisation that these objects preferentially lie on stellar streams and other debris features (Mackey et al. 2010b, 2013). Monte Carlo simulations indicate a probability of $\lesssim 1\%$ that such alignments should happen by chance, leading to the conclusion that 80% of the M31 outer halo GCs have been accreted along with their host galaxies, confirming the idea put forward by Searle & Zinn (1978) for the Milky Way. In this Letter, we present the first results of a spectroscopic survey of these outer halo objects, focusing on their global kinematics. A detailed description of the data as well as a full analysis is deferred for a later publication (Veljanoski et al. in prep).

2. THE DATA

Spectra were acquired for 53 GCs spanning $R_{proj} \sim 20-130$ kpc, of which 12(6) lie beyond $\gtrsim 80(100)$ kpc. This sample is complete down to $g \sim 18.5$, and 44 of the clusters had not previously been observed spectroscopically. The data were obtained over 15 nights during 2005-2010 using the ISIS spectrograph on the WHT 4.2m, and the RC spectrograph on the KPNO 4m. ISIS has two detectors that independently sample the blue and red spectral range. We used the R600B and R600R gratings to cover the wavelength range $\sim 350-510$ nm with a dispersion of 0.045 nm/pixel and $\sim 750-920$ nm with a dispersion of 0.079 nm/pixel respectively. With the RC spectrograph, we used the KPC007 grating with a wavelength coverage of $\sim 350-650$ nm and a dispersion of 0.139 nm/pixel. Total integrations were 600-7200 seconds depending on the target brightness. The slit width was $1-2''$. The signal-to-noise per pixel was $\approx 7-30$ for most targets and 50-70 for the brightest objects.

The data were reduced using standard IRAF¹² procedures.

¹² IRAF is distributed by the National Optical Astronomy Observatories, which are operated by the Association of Universities for Research in Astronomy, Inc., under cooperative agreement with the National Science Foundation

¹ Institute for Astronomy, University of Edinburgh, Royal Observatory, Blackford Hill, Edinburgh, EH9 3HJ, UK

² Research School of Astronomy & Astrophysics, Australian National University, Mt Stromlo Observatory, Weston Creek, ACT 2611, Australia

³ Astronomisches Rechen-Institut, Zentrum für Astronomie der Universität Heidelberg, Monchhofstr. 12-14, 69120 Heidelberg, Germany

⁴ Institute of Astronomy, University of Cambridge, Madingley Road, Cambridge, CB3 0HA, UK

⁵ NRC Herzberg Institute of Astrophysics, 5071 West Saanich Road, Victoria, British Columbia V9E 2E7, Canada

⁶ Department of Physics & Astronomy, University of Leicester, Leicestershire, LE1 7RH, UK

⁷ Observatoire de Strasbourg, 11, rue de l’Université, F-67000 Strasbourg, France

⁸ University of Massachusetts, Department of Astronomy, LGRT 619-E, 710 N. Pleasant Street, Amherst, Massachusetts, 01003-9305, USA

⁹ Institute of Astronomy, School of Physics, University of Sydney, NSW 2006, Australia

¹⁰ Max-Planck-Institut fuer Astronomie, Koenigstuhl 17, D-69117 Heidelberg, Germany

¹¹ Visiting Astronomer, Kitt Peak National Observatory, National Optical Astronomy Observatory, which is operated by the Association of Universities for Research in Astronomy (AURA) under cooperative agreement with the National Science Foundation.

One-dimensional spectra were extracted with aperture radii of 2-2.5". Heliocentric radial velocities were derived using a chi-squared minimization technique between GC spectra and radial velocity template stars (Veljanoski et al. 2013, in prep). This is analogous to the standard cross-correlation method, and it produces similar results. The method has the advantage that it uses the uncertainties in both the target and template spectra, which helps to eliminate spurious features in the chi-squared function.

The uncertainty in the radial velocity of each cluster is adopted to be the standard deviation of all the independent chi-squared minimizations between the cluster and multiple radial velocity standard stars. Furthermore, as we obtained two independent velocity measurements for the GCs observed with ISIS, these were combined to reduce the uncertainty in the final velocity value. The final median uncertainty of all 53 GC velocity measurements is 12 km/s. Of the 9 GCs in our sample that had published velocities in the RBC, all agree to within one standard deviation. Four of these clusters were found to have more precise RBC velocities compared to our measurements and for these we adopt the RBC values in our subsequent analysis.

As our GC sample spans a large extent on the sky, we converted our heliocentric radial velocities to the Galactocentric frame in order to remove any effects the Solar motion could have on the kinematics. This conversion was done using the relations presented in Courteau & van den Bergh (1999), with updated values for the Solar motion from McMillan (2011) and Schönrich et al. (2010). For the purpose of this study, we take the M31 heliocentric velocity to be -301 ± 4 km/s (Courteau & van den Bergh 1999), which translates to a Galactocentric radial velocity of -109 ± 4 km/s.

3. RESULTS

3.1. The Global Velocity Map

Figure 1 shows the most recent metal-poor ($[\text{Fe}/\text{H}] \lesssim -1.4$) red giant branch stellar density map from the Pan-Andromeda Archaeological Survey (PAndAS) (McConnachie et al. 2009). Overlaid are the positions of the observed GCs, the colors of which correspond to their measured Galactocentric radial velocities.

Three interesting groups of GCs are indicated on Figure 1. The blue rectangle marks 4 GCs that project on the North-West stream. A contiguous velocity gradient is seen along this feature, with the most radially-distant cluster ($R_{proj} \approx 125$ kpc) having a velocity of ≈ -183 km/s and the innermost object ($R_{proj} \approx 67$ kpc) having ≈ -380 km/s. Also marked (red contour) are the GCs that lie on stream D, a feature first identified by Ibata et al. (2007). There is no apparent velocity gradient in this case, but the velocities of the GCs observed in the northeastern part of the stream suggest two distinct kinematic groups. In particular, 4 GCs have a mean velocity and dispersion of -171 km/s and 50 km/s, while the remaining 3 GCs have mean velocity and dispersion of 71 km/s and 18 km/s. Interestingly, the northeastern part of stream D has been previously identified to be a complicated region where it overlaps stream C (Ibata et al. 2007; Richardson et al. 2011). Thus, it seems likely that the two kinematic GC groups we have identified are associated with these different streams, and are moving in the opposite sense around M31, as judged by their mean velocities. Radial velocities for stream stars in this overlapping region are not yet available, but the lone southern GC on stream D has a radial

velocity that lies within ~ 20 km/s of stream stars tentatively identified in a nearby field (Chapman et al. 2008). Interestingly, the And-I dwarf, located on the south end of Stream D, has a Galactocentric velocity of ~ -190 km/s, similar to one of the kinematic GC groups. The And-IX dwarf, located on the north end of Stream D with velocity of ~ -20 km/s, appears uncorrelated with the GC groups.

The yellow region on Figure 1 marks "association 2" which Mackey et al. (2010b) identified as a statistical overdensity of GCs not associated with any obvious underlying stellar debris feature. The spread of velocities indicates that not all of the GCs in this region can be members of a kinematically coherent subgroup. However, measurements for the remaining $\sim 60\%$ of the putative "association 2" GCs are required before the presence of a subgroup can be definitely ruled out.

3.2. Rotation and Velocity Dispersion

It has been known for some time that GCs in the inner regions of M31 rotate around the minor optical axis of the galaxy, in the same sense as the disk rotation. Perrett et al. (2002) measured a rotational amplitude of the GC system of ~ 140 km/s, while Lee et al. (2008) measured ~ 190 km/s using a larger sample. Dividing the GCs based on their metallicity, Deason et al. (2011) found more pronounced rotation for the metal-rich ($[\text{Fe}/\text{H}] > -1$) subpopulation. Inspection of Figure 1 strongly suggests this rotation persists to larger radii, with GCs in the northeast having systematically higher velocities than those in the southwest. Figure 2 shows the Galactocentric radial velocities, corrected for the systemic motion of M31, versus their projected distances along the M31 major axis. GCs belonging to the subgroups identified in Figure 1 are color-coded. The rotational signature appears to be a property of the bulk population of the outer halo GC sample and is not driven by one or two kinematically-coherent subgroups.

To further investigate the rotational signature, we follow Côté et al. (2001) and fit the observed projected Galactocentric radial velocities v_p of the GCs with the function,

$$v_p(\theta) = v_{sys} + A \sin(\theta - \theta_0) \quad (1)$$

where θ is the projected position angle, measured east of north, of a cluster relative to M31 center, θ_0 is the projected position angle of the GC system rotation axis, v_{sys} is the systemic velocity of the GC system and A is the amplitude of rotation. This approach assumes that the rotation axis of the GC system is perpendicular to the line of sight, and that the intrinsic angular velocity of the system is constant on spherical surfaces. The uncertainties are determined using the numerical bootstrapping technique (Efron 1982) and the derived rotational amplitudes are corrected for the inclination of the M31 disk, taken to be 77.5° (Ferguson et al. 2002).

We augment our radial velocities with those from the RBC and fit the GC sample as a whole as well as within and beyond 30 kpc. This radius corresponds to a clear break in the GC radial number density profile (Huxor et al. 2011) and therefore provides a natural division between the "inner" and "outer" halo. For reference, the outer halo sample consists of the 48 GCs presented here, to which we add a further 2 confirmed GCs from the RBC.

The systemic velocity of the GC system was set to the M31 Galactocentric systemic velocity. The results of this fitting are displayed in Table 1. The results remain unchanged when v_{sys} in Equation 2 is left to vary as a free parameter, or when the mean velocity of the GC system is used. Given the position

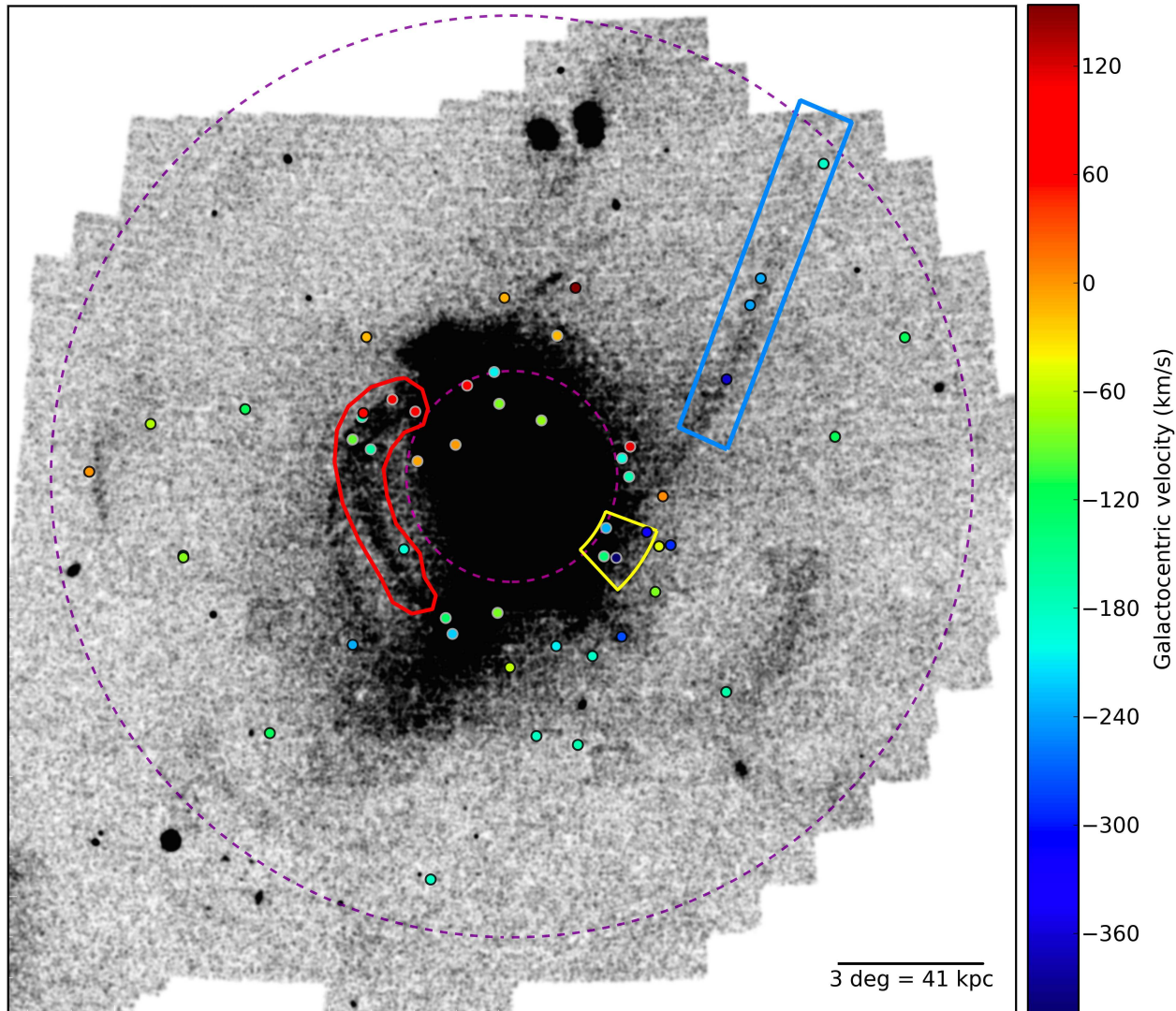


Figure 1. The metal-poor stellar density map of M31 from PAndAS. Positions of the observed GCs are marked with colored dots which correspond to their Galactocentric radial velocities in units of km/s. Some GC subgroups are indicated (see text for details). The purple dashed circles correspond to 30 and 130 kpc radii in projection. The Galactocentric velocity of M31 is -109 ± 4 km/s. North is up and East is left.

Table 1
Derived Rotational Properties for M31 Halo GCs

	A	θ_0	Velocity Dispersion	N_{GC}
	[km/s]	[degrees]	[km/s]	
All GCs	133 ± 11	124 ± 4	115 ± 5	595
$R_{proj} < 30$ kpc	137 ± 10	124 ± 4	114 ± 5	545
$R_{proj} > 30$ kpc	79 ± 19	123 ± 27	106 ± 12	50

angle of the M31 major axis is 38° , the derived rotation axis is consistent with the minor axis of M31, and is essentially indistinguishable from the rotation axis of the inner halo GCs.

Finally, we derived the rotation-corrected velocity dispersion of the M31 GC sample using the biweight scale of Beers et al. (1990). Figure 3 shows the rotation-corrected Galactocentric radial velocities (corrected for the systemic motion of M31) versus R_{proj} of the M31 GCs. It reveals a decreasing velocity dispersion with increasing distance from the M31 center, varying from ~ 122 km/s at 60 kpc to ~ 57 km/s at 120 kpc. For reference, the metal-poor field star velocity

dispersion is ~ 98 km/s at 60 kpc (measured), and ~ 44 km/s at 120 kpc (extrapolated) (Chapman et al. 2006).

3.3. An M31 Mass Estimate

Assuming the halo GC system is spherically symmetric, we can estimate the mass of M31 by solving the Jeans equation (Binney & Tremaine 1987). Because we have found evidence for rotation in the M31 halo GC system, the Jeans equation is separated into a rotating and a non-rotating component. The total mass is obtained by summing the mass supported by pressure M_p and the rotationally-supported mass M_r . The rotational component is determined via:

$$M_r = \frac{R_{max} v_{max}^2}{G} \quad (2)$$

where R_{max} is the projected radius of the outermost GC in our sample, v_{max} is the rotational amplitude of the outer GC population and G is the gravitational constant.

To determine M_p we use the solution of the non-rotating

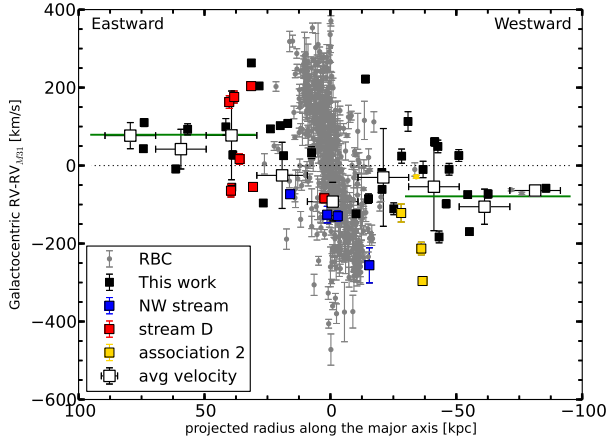


Figure 2. Galactocentric radial velocity, corrected for the M31 systemic motion, vs. projected radius along the M31 major axis. The black and colored squares mark the velocities of the GCs presented in this work, with different colors marking GC subgroups identified on Figure 1. RBC values are shown as small grey circles. The open squares correspond to the mean velocities of the GCs with $R_{proj} > 30$ kpc calculated in 20 kpc bins. The x error bars represent the bin size, while the y error bars indicate the standard deviation of the mean. The green solid lines correspond to our measured amplitude for the outer GCs corrected for inclination.

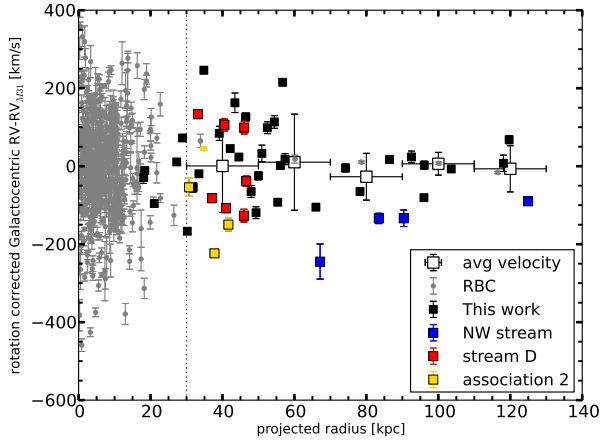


Figure 3. Rotation-corrected Galactocentric radial velocity, corrected for the M31 systemic motion, vs. R_{proj} from the M31 center. Symbols are as in Figure 1. The open squares correspond to the mean velocities of the halo clusters in 20 kpc bins. The x error bars mark the bin size, while the y error bars represent the rotation-corrected velocity dispersion. The dotted line marks the 30 kpc radius.

Jeans equation proposed by Evans et al. (2003), known as the tracer mass estimator (TME):

$$M_p = \frac{C}{GN} \sum_{i=1}^N (v_i - v_{sys})^2 R_i \quad (3)$$

where R_i is the projected radius from the center of M31 for a given cluster, v_i is the radial velocity of the GC with the rotational component removed and N is the total number of clusters in our sample. The constant C depends on the shape of the potential, the radial distribution of the tracer objects and the anisotropy in the system. For a spherical, isotropic

system, it has the following form:

$$C = \frac{4(\alpha + \gamma)}{\pi} \frac{4 - \alpha - \gamma}{3 - \gamma} \frac{1 - (r_{in}/r_{out})^{3-\gamma}}{1 - (r_{in}/r_{out})^{4-\alpha-\gamma}}. \quad (4)$$

In equation (4), r_{in} and r_{out} correspond to the smallest and largest 3D radii of the halo GCs respectively. In this case, we assume $r_{in} = 30$ kpc, while r_{out} is set to 200 kpc assuming MGC1 is the most remote GC (Mackey et al. 2010a). The constant α is related to the underlying gravitational field, which is assumed to be scale-free, at least between r_{in} and r_{out} . For an isothermal halo potential where the system has a flat rotation curve at large radii, α is zero. If we assume a NFW dark matter profile (Navarro et al. 1996), $\alpha \approx 0.55$ (Watkins et al. 2010). The γ parameter is the slope of the GC volume density distribution. We calculate this using the surface density distribution of all 84 GCs that have projected radii larger than 30 kpc (Huxor et al. 2013, in prep; Mackey et al. 2013, in prep) and find $\gamma \sim 3.34$. It is also important to note that even though the TME uses a GC sample in a shell around the center of M31, it calculates the total mass enclosed by the furthest cluster in that sample.

Using the above method, and setting α to zero, we calculate the total mass of M31 to be $M_{M31} = 1.5 \pm 0.2 \times 10^{12} M_{\odot}$, where the pressure component is $M_p = 1.3 \pm 0.2 \times 10^{12} M_{\odot}$ and the rotation contribution is $M_r = 2 \pm 1 \times 10^{11} M_{\odot}$. Assuming $\alpha = 0.55$, we find the M31 mass to be $M_{M31} = 1.2 \pm 0.2 \times 10^{12} M_{\odot}$, where $M_p = 1.0 \pm 0.2 \times 10^{12} M_{\odot}$ and $M_r = 2 \pm 1 \times 10^{11} M_{\odot}$. For reference, applying the TME in a single step (ignoring rotation), gives $M_{M31} = 1.8 \pm 0.2 \times 10^{12} M_{\odot}$ and $M_{M31} = 1.3 \pm 0.2 \times 10^{12} M_{\odot}$ for α values of 0 and 0.55 respectively. The quoted errors incorporate the statistical uncertainties only, and in reality they are much larger. In our mass calculations, we assume isotropic orbits, a steady state for our tracer population and a power-law form for the potential. This is the simplest approach we can take, although the presence of the substructure in the spatial distribution of the outer halo GCs suggests that it may not be correct. Nonetheless, studies suggest the presence of substructure in the tracer population will bias results only at the 20% level (e.g., Yenko et al. 2006; Deason et al. 2012). To explicitly test the assumption of steady state, we recalculate the M31 mass excluding GCs which lie along the North-West stream and stream D. We find the total mass of M31 decreases by $0.3 \times 10^{12} M_{\odot}$ for both values of α , with the formal statistical errors remaining unchanged.

4. DISCUSSION

Analysis of the radial velocities of M31 outer halo GCs strongly supports our earlier finding that many of these objects have been accreted (Mackey et al. 2010b). Clear kinematic correlations are seen amongst subgroups of GCs which lie on top of stellar debris features, and, in the case of the North-West stream, an unambiguous signature of radial infall is observed. Interestingly, recent work has also begun to detect phase-space substructure in large samples of GCs around distant galaxies (e.g. Strader et al. 2011; Blom et al. 2012; Romanowsky et al. 2012). However it is only within the Local Group that we can attempt the obvious next step of comparing GC velocities with those of underlying stream stars.

A surprising discovery is the high degree of rotation in the M31 outer halo GC population, which is in the same

sense as the inner halo population as well as the main stellar disk. While it is common to find GCs rapidly rotating in inner regions of galaxies, strong rotation beyond a few tens of kpc seems to be a rare occurrence, at least amongst early type galaxies (e.g. Woodley et al. 2010; Strader et al. 2011; Blom et al. 2012; Pota et al. 2013). It is natural to speculate on how such coherent motion could arise if the outer GC population were largely accreted from numerous dwarf galaxy hosts. One possibility is that the donor dwarf galaxies have been accreted from a few preferred directions on the sky and hence have aligned angular momenta, as seen in some recent cosmological simulations (Libeskind et al. 2005, 2011; Lovell et al. 2011). Such a scenario has also been suggested as the origin of the planar alignments of dwarf galaxies seen in both the Milky Way and M31 (e.g. Metz et al. 2007; Ibata et al. 2013). Curiously, the plane of dwarf galaxies reported in M31 rotates in the same sense as the outer halo GC population, although the rotation axis of that plane appears to be inclined by ~ 45 deg to the minor axis. It is also possible that the bulk of the M31 outer halo GC population was accreted in a single event involving a moderate mass satellite. Support for this idea could come from the M31 thick disk which rotates in the same sense, albeit somewhat faster, than the halo GC population (Collins et al. 2011). However, a rather massive satellite would be required to bring in a population of several tens of GCs, raising the question of how the M31 disk could survive such an encounter. Furthermore, it would seem difficult to explain the spatial correlation between outer halo GCs and the numerous tidal streams in this case. In a different scenario, numerical modelling (Bekki 2010) suggests that a past major merger between M31 and another disk galaxy could give rise to the rapid rotation of the resulting GC system, including the rotation in the halo population.

Despite being our closest massive galaxy, it is remarkable that we are still unable to measure the total mass of M31 with good precision. Indeed, there is still debate as to whether M31 or the Milky Way is more massive (Watkins et al. 2010). Evans et al. (2003) used GC kinematics to find a M31 mass of $1.2 \times 10^{12} M_{\odot}$ out to a deprojected 3D distance of ~ 100 kpc, while Galletti et al. (2006) and Lee et al. (2008) used expanded samples to calculate masses of $1.9 - 2.4 \times 10^{12} M_{\odot}$ within the same radial range. Several authors have attempted to determine the M31 mass via the motions of its dwarf satellite galaxies (e.g. Côté et al. 2000; Evans et al. 2003). The most recent such measurement is presented by Watkins et al. (2010) who estimated $1.4 \pm 0.4 \times 10^{12} M_{\odot}$ using 23 satellites out to 300 kpc, assuming isotropy. Our estimate of $M_{M31} = 1.2 - 1.5 \pm 0.2 \times 10^{12} M_{\odot}$ within a 3D radius of 200 kpc agrees well with this value but suffers from the similar systematic uncertainties due to model assumptions. Notably, van der Marel et al. (2012) use the velocity vector of M31 with respect to the Milky Way in combination with the timing argument to derive a total mass for the Local Group $M_{LG} = (4.39 \pm 1.63) \times 10^{12} M_{\odot}$, which would push the M31 mass higher than any estimate thus far using dynamical tracers.

ADM is supported by ARC grant DP1093431. APH was partially supported by Sonderforschungsbereich SFB 881 "The Milky Way System" of the German Research Foundation. The WHT is operated on the island of La Palma by the Isaac Newton Group in the Spanish Observatorio del Roque

de los Muchachos of the Instituto de Astrofísica de Canarias. *Facilities:* KPNO (RC-spectrograph) WHT (ISIS-spectrograph).

REFERENCES

- Beers, T. C., Flynn, K., & Gebhardt, K. 1990, *AJ*, 100, 32
 Bekki, K. 2010, *MNRAS*, 401, L58
 Binney, J., & Tremaine, S. 1987, Princeton, NJ, Princeton University Press, 1987, 747 p.,
 Blom, C., Forbes, D. A., Brodie, J. P., et al. 2012, *MNRAS*, 426, 1959
 Brodie, J. P., & Strader, J. 2006, *ARA&A*, 44, 193
 Chapman S. C., Ibata R., Lewis G. F., Ferguson A. M. N., Irwin M., McConnachie A., Tanvir N., 2006, *ApJ*, 653, 255
 Chapman, S. C., Ibata, R., Irwin, M., et al. 2008, *MNRAS*, 390, 1437
 Collins M. L. M., et al., 2011, *MNRAS*, 413, 1548
 Côté, P., Mateo, M., Sargent, W. L. W., & Olszewski, E. W. 2000, *ApJ*, 537, L91
 Côté, P., McLaughlin, D. E., Hanes, D. A., et al. 2001, *ApJ*, 559, 828
 Courteau, S., & van den Bergh, S. 1999, *AJ*, 118, 337
 Deason, A. J., Belokurov, V., Evans, N. W., et al. 2012, *MNRAS*, 425, 2840
 Deason, A. J., Belokurov, V., & Evans, N. W. 2011, *MNRAS*, 411, 1480
 Efron, B. 1982, *CBMS-NSF Regional Conference Series in Applied Mathematics*, Philadelphia: Society for Industrial and Applied Mathematics (SIAM), 1982,
 Evans, N. W., Wilkinson, M. I., Perrett, K. M., & Bridges, T. J. 2003, *ApJ*, 583, 752
 Ferguson, A. M. N., Irwin, M. J., Ibata, R. A., Lewis, G. F., & Tanvir, N. R. 2002, *AJ*, 124, 1452
 Forbes, D. A., Brodie, J. P., & Grillmair, C. J. 1997, *AJ*, 113, 1652
 Galletti, S., Federici, L., Bellazzini, M., Fusi Pecci, F., & Macrina, S. 2004, *A&A*, 416, 917
 Galletti, S., Federici, L., Bellazzini, M., Buzzoni, A., & Fusi Pecci, F. 2006, *A&A*, 456, 985
 Huxor, A. P., Tanvir, N. R., Irwin, M. J., et al. 2005, *MNRAS*, 360, 1007
 Huxor, A. P., Tanvir, N. R., Ferguson, A. M. N., et al. 2008, *MNRAS*, 385, 1989
 Huxor, A. P., Ferguson, A. M. N., Tanvir, N. R., et al. 2011, *MNRAS*, 414, 770
 Ibata, R., Martin, N. F., Irwin, M., et al. 2007, *ApJ*, 671, 1591
 Ibata, R. A., Lewis, G. F., Conn, A. R., et al. 2013, *Nature*, 493, 62
 Lee, M. G., Hwang, H. S., Kim, S. C., et al. 2008, *ApJ*, 674, 886
 Libeskind, N. I., Frenk, C. S., Cole, S., et al. 2005, *MNRAS*, 363, 146
 Libeskind, N. I., Knebe, A., Hoffman, Y., et al. 2011, *MNRAS*, 411, 1525
 Lovell, M. R., Eke, V. R., Frenk, C. S., & Jenkins, A. 2011, *MNRAS*, 413, 3013
 Mackey, A. D., Ferguson, A. M. N., Irwin, M. J., et al. 2010a, *MNRAS*, 401, 533
 Mackey, A. D., Huxor, A. P., Ferguson, A. M. N., et al. 2010b, *ApJ*, 717, L11
 Mackey, A. D., Huxor, A. P., Ferguson, A. M. N., et al. 2013a, *MNRAS*, 429, 281
 van der Marel, R. P., Fardal, M., Besla, G., et al. 2012, *ApJ*, 753, 8
 McConnachie, A. W., Irwin, M. J., Ferguson, A. M. N., et al. 2005, *MNRAS*, 356, 979
 McConnachie, A. W., Irwin, M. J., Ibata, R. A., et al. 2009, *Nature*, 461, 66
 McMillan, P. J. 2011, *MNRAS*, 414, 2446
 Metz, M., Kroupa, P., & Jerjen, H. 2007, *MNRAS*, 374, 1125
 Navarro, J. F., Frenk, C. S., & White, S. D. M. 1996, *ApJ*, 462, 563
 Perrett, K. M., Bridges, T. J., Hanes, D. A., et al. 2002, *AJ*, 123, 2490
 Pota, V., Forbes, D. A., Romanowsky, A. J., et al. 2013, *MNRAS*, 428, 389
 Richardson J. C., et al., 2011, *ApJ*, 732, 76
 Romanowsky A. J., Strader J., Brodie J. P., Mihos J. C., Spitler L. R., Forbes D. A., Foster C., Arnold J. A., 2012, *ApJ*, 748, 29
 Searle, L., & Zinn, R. 1978, *ApJ*, 225, 357
 Schönrich, R., Binney, J., & Dehnen, W. 2010, *MNRAS*, 403, 1829
 Strader, J., Romanowsky, A. J., Brodie, J. P., et al. 2011, *ApJS*, 197, 33
 Watkins, L. L., Evans, N. W., & An, J. H. 2010, *MNRAS*, 406, 264
 West, M. J., Côté, P., Marzke, R. O., & Jordán, A. 2004, *Nature*, 427, 31
 Woodley, K. A., Gómez, M., Harris, W. E., Geisler, D., & Harris, G. L. H. 2010, *AJ*, 139, 1871
 Yenko B. M., Johnston K. V., Bullock J. S., Rhode K. L., 2006, *ApJ*, 643, 154
 di Tullio Zinn, G., & Zinn, R. 2013, *AJ*, 145, 50